Combination of GNSS and InSAR measured at co-located geodetic monitoring sites

Thomas Fuhrmann and Matthew Garthwaite

Geodesy Section, Community Safety and Earth Monitoring Division, Geoscience Australia, Australia
E-Mail: thomas.fuhrmann@ga.gov.au, matt.garthwaite@ga.gov.au

Abstract

Global Navigation Satellite Systems (GNSS) can provide a temporally dense set of geodetic coordinate observations in three dimensions at a limited number of discrete measurement points on the ground. Compared to this, the Interferometric Synthetic Aperture Radar (InSAR) technique gives a spatially dense set of geodetic observations of ground surface movement in the viewing geometry of the satellite platform, but with a temporal sampling limited to the orbital revisit of the satellite. Using both of these methods together can leverage the advantages of each to derive more accurate, validated surface displacement estimates with both high temporal and spatial resolution. In this paper, we discuss the properties of both techniques with a view to combined usage for improving future national datums. We apply differential GNSS processing to data observed at a local geodetic network in the Sydney region as well as time series InSAR analysis of Radarsat-2 data. We compare and validate surface displacements resulting from the two techniques at 21 geodetic monitoring sites equipped with GNSS and radar corner reflectors (CRs). The resulting GNSS/InSAR displacement time series agree at the level of 5 to 10 mm. This case study shows that co-located GNSS/CR sites are well-suited to compare and combine GNSS and InSAR measurements. An investigation of potential multipath effects introduced by the CRs attached directly to GNSS monumentation found that daily site coordinates are affected at a level below 0.1 mm. The GNSS/CR sites may hence serve as a local tie for future incorporation of InSAR into national datums. This will allow frequent updates of national geodetic networks and corresponding datums by using the large-scale and spatially dense information on surface displacements resulting from InSAR analyses.

1 Introduction

National geodetic networks consist of a set of fixed benchmarks (or reference sites) and provide a country with coordinates to form a national datum (Heck, 2003). Current horizontal datums usually consider the general movement trend of tectonic plates measured with Global Navigation Satellite Systems (GNSS), but usually do not account for local deformation of the Earth's surface. Vertical datums are usually based on levelling and gravity measurements to provide physical heights at fixed benchmarks. Often, the benchmark heights are not frequently re-measured and may become outdated where local deformation causes surface movements. The source of local deformation can be natural (e.g. intra-plate tectonics, landslides or groundwater changes) or anthropogenic (e.g. subsurface mining or construction activities) and induce horizontal and vertical coordinate changes with magnitudes of several millimetres to metres.

Heckmann et al. (2015) state that benchmark coordinates, heights and gravity values are generally time-dependent values. Currently, the only way to up-

Erschienen bei KIT Scientific Publishing
Schriftenreihe des Studiengangs
Geodäsie und Geoinformatik 2018,1

DOI Einzelbeitrag:
10.5445/KSP/1000080215

Festschrift zur Verabschiedung von
Prof. Dr.-Ing. Dr. h.c. Bernhard Heck
(Schw)Ehre, wem (Schw)Ehre gebührt

DOI Festschrift:
10.5445/KSP/1000080324

date benchmark coordinates affected by surface deformation is to re-measure the coordinates by conducting a repeat GNSS or levelling survey. This is a time-consuming and costly exercise. In this paper, we propose the use of satellite radar remote sensing to characterise local surface deformation, and to update coordinates and datums on a routine basis. Interferometric Synthetic Aperture Radar (InSAR) is a satellite remote sensing technique which enables the detection of millimetre-scale movements of the Earth's surface over large areas. In contrast to the point-wise information provided by GNSS or levelling, InSAR can cover large areas with a high spatial density of observations and, therefore, is well-suited to cover the spatial scales of surface deformation phenomena. High accuracy in the horizontal coordinate and displacement components is obtained from GNSS, whereas InSAR is more sensitive to vertical surface displacements. Combining the two techniques can therefore take advantage of their complementary properties with respect to spatial and temporal resolution as well as sensitivity to different displacement components.

The primary objective of the work presented here is to investigate the potential for improving the spatial and temporal resolution of geodetic datums by routinely combining these independent geodetic data in the future. We present a case study in which we analyse data acquired since July 2016 from a local network of 21 geodetic monitoring sites in the Sydney region, covering an area of about 20 km x 20 km. Each site consists of a co-located GNSS monument and two radar corner reflectors (CRs), which reflect the radar signal back to the satellite with a high signal-to-noise ratio for exploitation in the InSAR analysis. These geodetic monitoring sites demonstrate that InSAR measures the same deformation signal as GNSS and, serve as a proof of concept that co-location of GNSS/InSAR CRs provides opportunity to conduct a local tie between the techniques.

2 Geodetic methods

This section gives a brief overview of how surface displacements are derived from GNSS and InSAR data as well as the major characteristics of both geodetic techniques. Some remarks on using radar CRs and local ties between GNSS and InSAR at co-located sites are included in sub-Section 2.3.

2.1 Surface displacements from GNSS

Three-dimensional (3D) position coordinates are estimated from multiple GNSS observations over a certain time period, e.g. one daily coordinate estimate from 24 hours of GNSS observations. Surface displacements are subsequently derived as a change of position over time. A relative (or differential) positioning strategy enables most of the perturbation terms affecting GNSS signals to be eliminated, or at least reduced, by combining observations of different satellites and receivers at different measurement epochs (e.g. Hofmann-Wellenhof et al., 2008). Differential GNSS analyses make use of a network of surrounding reference sites and are suitable to estimate coordinates of a local network at high precision (Torge and Müller, 2012). The GNSS data presented in Section 3.2 were analysed as a differential network using a stochastic connection to surrounding International GNSS Service (IGS) sites[1], and surrounding Asia Pacific Reference Frame (APREF) sites[2]. The results are daily geocentric coordinates (XYZ) at each site in ITRF2014 (Altamimi et al., 2016).

The major displacement trend follows the movement vector of the Australian tectonic plate across the area of interest. In order to obtain local deformation, the linear trend is calculated at each GNSS site from an Australian tectonic plate model (see ICSM, 2017) and subtracted from the XYZ coordinate time series. Subsequently, XYZ coordinates are transformed to longitude, latitude and ellipsoidal height. The first daily coordinate estimate serves as a temporal reference and is set to zero. Finally the longitude, latitude and height differences with respect to the first day are transformed to topocentric metric coordinate differences (East, North, Up) using the local radii of curvature of the Ellipsoid. Table 2.1 summarises the characteristics of surface displacements derived from GNSS using the described method. Note that precision of the Up component of displacement is a factor of three poorer

[1] Seven sites located on the Australian tectonic plate.
[2] Ten sites at distances between 30 and 200 km from the area of interest.

Table 2.1: Characteristics of GNSS and InSAR with respect to surface displacement estimation; values given in brackets for spatial and temporal resolution of InSAR relate to the Radarsat-2 data used within this paper

	Temporal resolution	Spatial resolution	Spatial reference	Precision	Sensitivity to East, North, Up displacem.
GNSS:	high: daily (for continuously operating sites)	low: point-wise, at least several km between points	reference sites used for differential processing	high: 1 mm horizontal, 3 mm vertical	high, high, medium
InSAR:	medium: weeks to months (24 days)	high: pixel size of the sensor (9 m x 9 m pixels)	reference area, often chosen arbitrarily	medium: 3-6 mm (for C-band sensors)	medium, low, high

than the horizontal components. This is because visible GNSS satellites are only distributed in the hemisphere above the local horizon (e.g. Choi et al., 2007).

2.2 Surface displacements from InSAR

Spaceborne synthetic aperture radar (SAR) systems measure the range (i.e. the distance to the detected object) and the intensity of radar backscattering from the ground surface. From their side-looking image geometry, SAR sensors provide a 2D map of the Earth's surface in the coordinate system of the platform. As for GNSS, the distance to an object is expressed by a phase measurement. InSAR is a processing technique that makes use of two or more SAR images acquired at different times to derive relative surface displacements from changes in the measured phase signal. When a stack of SAR data is available, images of phase difference are calculated (so-called "interferograms"), resulting in a displacement time series for each image pixel. However, the phase information may be noisy at some pixels if the backscattering characteristics of the ground change through time (this phenomenon is particularly apparent in vegetated areas). Ferretti et al. (2000, 2001) introduced the concept of Persistent Scatterer (PS) InSAR (PS-InSAR) processing, which makes use of a subset of pixels with consistent backscattering through time. At selected PS pixels the phase signal is analysed and other nuisance terms contributing to the signal, such as atmospheric or orbital effects, are separated from the phase signal with the remainder assumed to be related to surface displacement (e.g. Hooper et al., 2004; Hooper et al., 2007; Adam et al., 2003; Kampes, 2005). The displacement signal is subsequently transformed to a metric displacement using the wavelength of the radar sensor. Common radar wavelengths used by SAR satellite sensors are 3.1 cm (X-band), 5.6 cm (C-band) and 23.6 cm (L-band).

As for GNSS displacement analysis, a spatial and temporal reference must be defined during the processing. In the case of InSAR, the spatial reference must be located within the imaged area. It is common practice to choose an area presumed to be stable and containing several hundreds to thousands of PS pixels. All displacements can then be interpreted relative to this presumably stable reference area. The temporal reference is restricted to the SAR image acquisition dates. As for GNSS, the first acquisition of a given image stack can be used as a temporal reference. Table 2.1 summarises the characteristics of surface displacements derived from PS-InSAR. Note that displacements from InSAR are measured along a slanted, 1D line of sight (LOS) towards the satellite. Radar satellites acquire image data of the same area on ascending (travelling south to north) and descending (travelling north to south) orbital passes. When information from both orbital viewing geometries is present, LOS displacements can be mathematically transformed to East-West and Up-Down components of the 3D displacement field. Sensitivity to North-South displacements is low due to the polar orbit of all SAR satellites and the side-looking image geometry.

In order to derive horizontal and vertical displacement components from InSAR, we combine the displacement data observed in ascending and descending image geometries. This is possible if LOS displacements are available (i) at the same location for all analysed tracks and (ii) within the same time period. To fulfil (i), spatial interpolation is needed as the location of PS pixels is different for each analysed stack of images. The Kriging technique (e.g. Li and Heap, 2008)

is applied to interpolate LOS displacements to a common grid taking into account the geostatistical properties of the displacements at each measurement epoch. By combining displacement rates (i. e. velocities) resulting from linear regression of the displacement time series at each pixel, no temporal reference is needed. Combination of epoch displacements instead of linear rates would require interpolation in time in addition to the spatial interpolation. The conversion of LOS displacement rates from one ascending and one descending geometry can only solve for vertical and one horizontal component (East-West), since InSAR is insensitive to displacements in the North-South direction. Therefore, we solve for Up-Down and East-West velocities (v_E and v_U, respectively) by inversion of

$$\begin{pmatrix} V_{asc} \\ V_{desc} \end{pmatrix} = \begin{pmatrix} -\sin\theta_{asc}\cos\alpha_{asc} & \cos\theta_{asc} \\ -\sin\theta_{desc}\cos\alpha_{desc} & \cos\theta_{desc} \end{pmatrix} \cdot \begin{pmatrix} v_E \\ v_U \end{pmatrix} \tag{2.1}$$

at each pixel with given ascending and descending LOS velocities (V_{asc} and V_{desc}, respectively) and corresponding incidence angle θ and satellite heading α. Equation 2.1 implicitly assumes no displacement in North-South direction is measurable by InSAR. This assumption is valid in most cases since only a small fraction of a North-South-oriented displacement would map into the InSAR LOS geometry. From the projection vectors of East, North and Up components of deformation into the LOS geometry, a sensitivity decomposition can be derived (Samieie-Esfahany et al., 2010). For θ and α of the ascending or descending Radarsat-2 data used in our case study (Section 3) the sensitivity decomposition of deformation results in values of 0.60, 0.18 and 0.78 for the East, North and Up component, respectively. Hence, any North-South deformation will have significantly less influence on the resulting combined displacement rates (East and Up components). However, neglecting East-West deformation by converting LOS displacements from one direction only (ascending or descending) into vertical displacements would result in incorrect estimates as the East-West component has a strong contribution to the LOS geometry. For more information on spatial interpolation of InSAR displacements at PS pixels and data combination see Fuhrmann et al. (2015a) and Fuhrmann (2016).

2.3 Co-located GNSS/InSAR measurements using Radar corner reflectors

Generally, the exact position of radar backscattering within a PS pixel is unknown and the total signal response is usually due to contributions from many scatterers within the pixel. However, artificial targets designed to backscatter a high proportion of incident radar energy, such as radar corner reflectors (CRs), enable the absolute position of a PS pixel to be known. CRs can therefore be used to validate and combine InSAR with other geodetic techniques for surface displacement analysis. Furthermore, geodetic monitoring sites consisting of a GNSS antenna and a CR may serve as a local tie to connect InSAR observations into national datum determination. National networks of GNSS sites provide a large-scale absolute reference frame which could be densified using information on local deformation derived from InSAR, in the future. In this case the local tie of GNSS and InSAR connects relative displacements derived from InSAR on adjacent satellite tracks to the national GNSS (and other geodetic) networks that are used to derive displacements.

Figure 2.1: Geodetic monitoring site CA19 consisting of GNSS antenna/receiver and two CRs aligned for ascending and descending passes of Radarsat-2

Figure 2.1 shows an example of a co-located geodetic monitoring site (CA19) as used in the case study described in Section 3. GNSS observations are acquired continuously at CA19. The CRs are oriented for SAR signals transmitted by the Radarsat-2 satellite on ascending and descending orbital passes with a repeat time of 24 days on each pass. A CR reflects incoming radar energy back to the SAR sensor by way of a

triple bounce reflection off the three orthogonal reflector plates. The amount of energy reflected to the SAR sensor depends on the size, shape and material of the reflector as well as on the orientation of the reflector with respect to the transmitted radar signal. The deployed CRs have square reflector panels, 60 x 60 cm. A detailed description of suitable sizes of CRs for use with commonly employed SAR frequencies as well as considerations with respect to manufacturing and long-term installation of these artificial targets is given by Garthwaite et al. (2015) and Garthwaite (2017).

The received signal from a CR in a certain InSAR dataset depends on the magnitude of the signal returned from the CR, but also the summed signal from all the other scatterers within the imaged pixel. The latter component of the received signal is referred to as clutter. The level of clutter in the vicinity of the deployed CR has a detrimental effect on the level of noise in phase observations. The Signal-to-Clutter Ratio (SCR) is therefore a quantity that can be used to determine the likely quality of PS-InSAR observations originating from a deployed CR.

SCR values calculated at the CRs of site CA19 for the period of Radarsat-2 acquisitions in the case study area (since July 2015) are shown in Figure 2.2 for SAR data acquired on both ascending and descending passes. Although some seasonal variability is evident, the SCR at CA19 is generally above 20 dB for the period between July 2016 (when the geodetic monitoring site was established) and November 2017 compared to the period before CR installation. The SCR is also generally above 20 dB at all other CRs in the geodetic network. The level of phase noise expected in C-band SAR data for an SCR of 20 dB is approximately 0.3 mm (Garthwaite, 2017), which is a small fraction of any deformation signal of interest. We therefore judge our CR design to be suitable for the Radarsat-2 data used and the environmental conditions in the vicinity of the geodetic monitoring sites. At some CRs, we observe a sudden decrease of SCR values, which can be related to damage and/or misalignment of the CR. Monitoring the SCR is therefore a useful way to remotely detect potential issues at monitoring sites that can then be quickly fixed in the field.

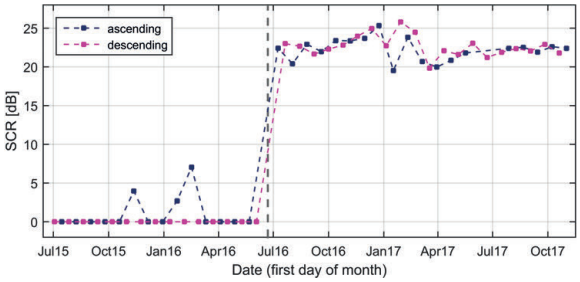

Figure 2.2: SCR values (given in dB, with linear-scale SCR values below 1 set to 0 dB) derived from ascending and descending Radarsat-2 data captures of the CRs at site CA19; the time of CR deployment is indicated by the vertical dashed gray line

3 Case study in the Sydney region

This section presents the case study to combine surface displacements from GNSS and InSAR in the Sydney region of New South Wales (NSW), Australia. The case study area and database are described (Section 3.1) as well as the displacement results (Section 3.2). Section 3.3 presents the results of an investigation in to the potential multipath effects that could be introduced by CRs attached directly to GNSS monumentation.

3.1 Case study area and database

The studied area and the available datasets are shown in Figure 3.1. Radarsat-2 data were acquired on one ascending and one descending track with a 24 day repeat time since July 2015. Figure 3.1 also displays the GNSS sites located within the area of interest. Three of the sites are part of CORSnet-NSW GNSS network operated by NSW Spatial Services, (i.e. sites CRDX, PCTN and MENA). In cooperation with NSW Spatial Services, CRs were attached to the GNSS monument at site MENA in June 2016 (see Section 3.3). In addition, 20 new geodetic monitoring sites were established in May 2016 consisting of the setup shown in Figure 2.1. Most of these new sites are operated on a campaign basis, with 24 hours of GNSS observations being acquired at monthly intervals since July 2016. Four of the new sites are operated continuously.

3.2 Results: surface displacements

The GNSS database is analysed as described in Section 2.1 using the Bernese GNSS Software (Dach et al., 2015) to calculate XYZ coordinates for each site and each analysed day. Note that for consistency with

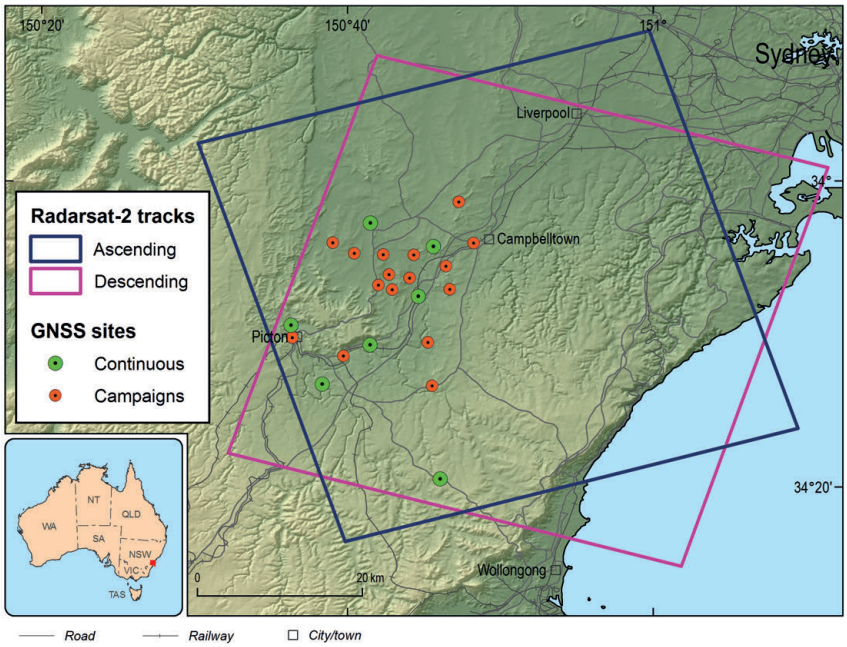

Figure 3.1: Overview of the database: GNSS sites and SAR tracks in ascending and descending geometries; Background: Digital Elevation Model

the surrounding reference network, only data from the Global Positioning System (GPS) have been analysed to estimate daily site coordinates. Figure 3.2 displays the resulting coordinate time series at continuously operating site CA19 after subtraction of the general trend of the Australian Plate.

This site is affected by strong horizontal motion particularly at the beginning of the time series. The total horizontal displacement sums to about 5 cm in the Southeasterly direction. The resulting coordinate time series for the Up component is noisier than the East and North components. This is because vertical coordinate estimates and corresponding coordinate changes are less accurate compared to horizontal coordinate estimates. Despite this, a slight downward displacement trend totalling about 1.5 cm can be observed at CA19. Mean coordinate standard deviations (2σ) are 1.1 mm

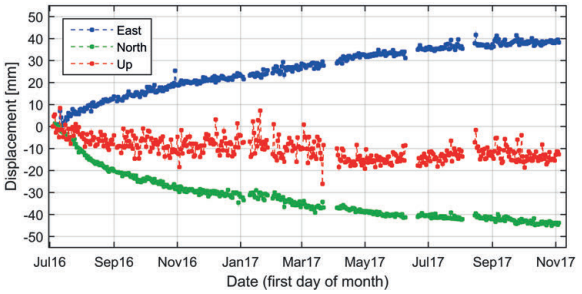

Figure 3.2: Displacement (i.e. coordinate changes in East, North and Up component) at site CA19 with respect to the first observed epoch (4 July 2016)

and 2.9 mm for horizontal and vertical components, respectively. Although all three dimensions of the displacement vector can be observed from GNSS analysis, only 1D information in the LOS is provided by a single InSAR analysis. However, instead of a pointwise displacement, InSAR is able to provide a spatially dense image of surface displacements. Figure 3.3 displays linear displacement rates (i.e. velocities) for the area of interest derived from separate PS-InSAR analyses, as described in Section 2.2, for the ascending and descending Radarsat-2 tracks between July 2015 and November 2017. Note that the displacements are observed along the slanted LOS towards the satellite which is different for the ascending and descending image geometries: the ascending pass observes the ground at an angle of 38.6° against the vertical, looking towards the east; the descending pass at an angle of 38.6° against the vertical, looking towards the west. The LOS displacement rates shown in Figure 3.3 are relative to an arbitrarily chosen reference area located in western Sydney. Note that the same reference area was used for InSAR analyses in both tracks in order to enable a consistent combination of ascending and descending displacement data. Mean standard deviations (2σ) of linear velocities are 1.0 mm/yr and 0.7 mm/yr for the ascending and descending passes, respectively.

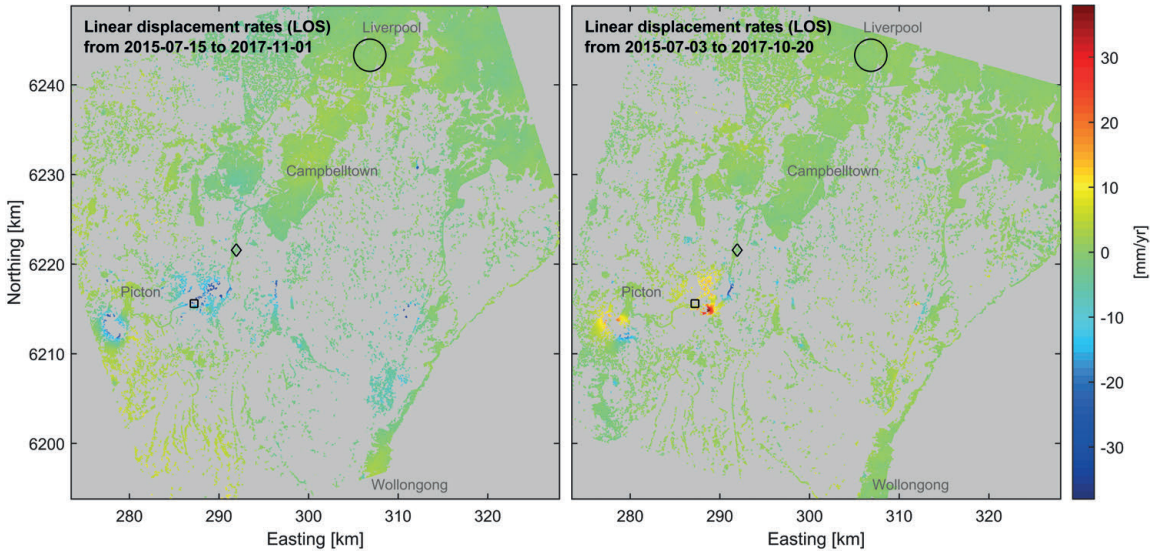

Figure 3.3: LOS displacement rates from analysis of ascending (left image) and descending (right image) Radarsat-2 data; the black circle marks the reference area, the black square and diamond mark the location of site CA19 and MENA, respectively

The LOS displacement rates shown in Figure 3.3 are interpolated to a 50 m grid, where interpolation is only performed if a certain number of PS pixels is available in the surroundings of a given interpolation location. The time period of the available Radarsat-2 data is roughly the same for both tracks. The two LOS datasets are, therefore, suitable for combination to vertical and East-West displacement rates using Equation 2.1 as described in Section 2.2. From the resulting velocity fields shown in Figure 3.4 (East-West and Up-Down components) one can state that the northern part of the analysed area was stable in the period between July 2015 and November 2017 within ± 2 mm/yr (green colours) and that several significant movements with velocities of up to 30 mm/yr occurred in the area south-west of Sydney. The combined results shown in Figure 3.4 demonstrate how PS-InSAR can deliver a spatially dense dataset of horizontal and vertical surface displacement observations, particularly when applied in urban areas, such as Sydney, where PS pixel density is high.

The geodetic monitoring sites enable the comparison of the displacements derived from GNSS and InSAR at the same measurement location. Figure 3.5 shows the LOS displacements at site CA19 (pictured in Figure 2.1) resulting from analysis of Radarsat-2 data since July 2016. By that time, the CRs had been installed and show reasonable SCR values (see Figure 2.2). For validation, we project the 3D displacement changes resulting from GPS analysis into the ascending and descending LOS of the corresponding Radarsat-2 track. For the descending geometry there is a good fit between the InSAR and GPS displacements. Note that the GPS displacements are noisier compared to InSAR because of the strong influence of the GPS-derived Up component on the projected LOS displacement vector. For the ascending LOS the fit between GPS and InSAR is good for the first 10 months of the time series, becoming slightly worse after April 2017. This discrepancy is possibly due to un-modelled phase contributions present in the ascending pass InSAR data and could improve with the acquisition of more InSAR data.

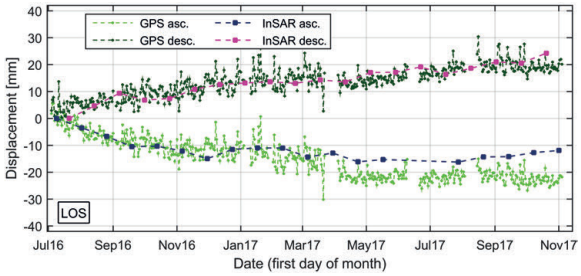

Figure 3.5: LOS displacements measured at site CA19 by InSAR at ascending (asc.) and descending (desc.) CRs and by GPS at the antenna on top of the pole (see 2.1); GPS East, North and Up components are projected into ascending and descending LOS geometry.

Similar results for the agreement between GNSS and InSAR are observed at other geodetic monitoring sites in the network. A statistical assessment of LOS displacements derived by InSAR and GNSS at the 21 GNSS sites equipped with CRs results in an average

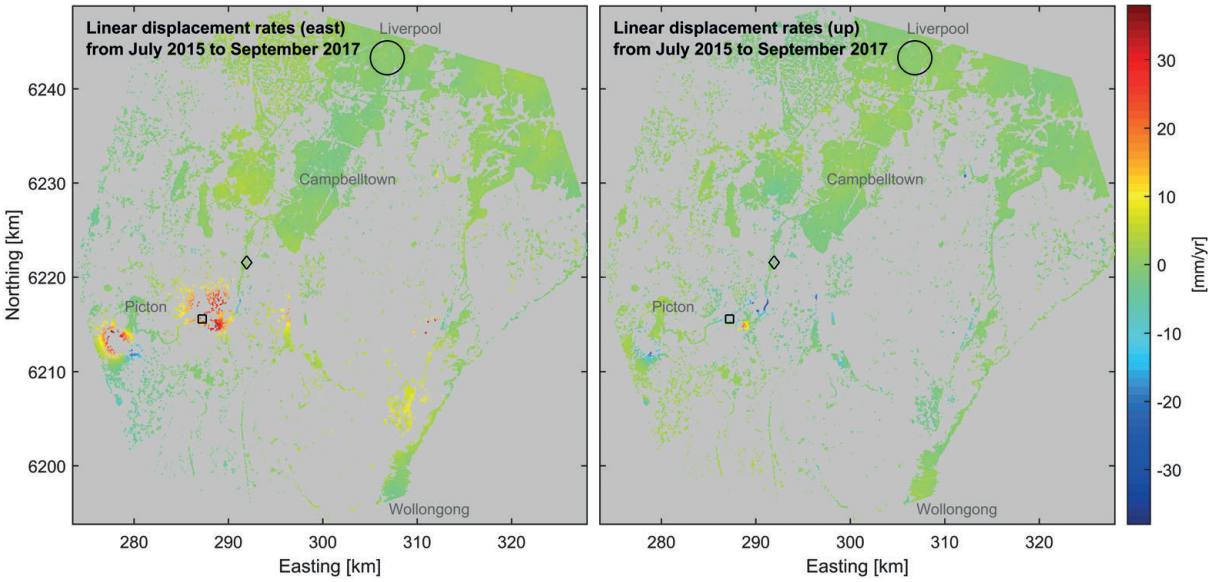

Figure 3.4: Displacement rates from combination of ascending and descending Radarsat-2 tracks, left: East component, right: Up component; the black circle marks the reference area, the black square and diamond mark the location of site CA19 and MENA, respectively

difference of 4.8 mm and 4.2 mm for the ascending and descending LOS, respectively, with most differences being within 10 mm (maximum difference of 20 mm). Consequently, we can state that displacements measured by both techniques agree at the level of 5 to 10 mm at our geodetic monitoring sites, but CA19 is the only site in the analysed geodetic network affected by surface displacement greater than 10 mm in magnitude.

Figure 3.6: Site MENA before (left image) and after (right image) radar CRs were attached to the antenna pole

3.3 GNSS multipath caused by co-located corner reflectors

Multipath effects, caused by reflections in the near- and far-fields of a GNSS antenna, distort the originally transmitted GNSS signal through interference. As a consequence, all objects surrounding a GNSS antenna can potentially be sources of multipath. Hence, the CRs attached directly to the GNSS monument are likely to induce some kind of multipath to observed GNSS signals. At site MENA (Menangle, NSW, see Figure 3.6), GNSS data had been acquired for over three years prior to the attachment of the CRs on 25 May 2016. This site is therefore suitable to assess the effect of potential GNSS signal interference with the CRs.

We compare coordinate variability and standard deviations resulting from daily GPS processing from the periods before and after CRs were attached at the site. A similar investigation has been performed by Parker et al. (2017) for CRs which are located several tens of metres away from a continuous GNSS site. For this scenario, no detectable increase in the average RMS of GNSS carrier-phase residuals was found, when comparing the residuals before and after CRs were deployed. At MENA and the other geodetic monitoring sites in the area, the CRs are mounted directly underneath the GNSS antenna and could therefore affect GNSS observations more significantly.

Figure 3.7, left image, displays the time series of coordinate changes at site MENA since January 2013 for the East component of displacement. In order to assess the effect of the CRs on the coordinate estimates, we calculate the mean absolute difference with respect to a moving average for each analysed day (red line in Fig-

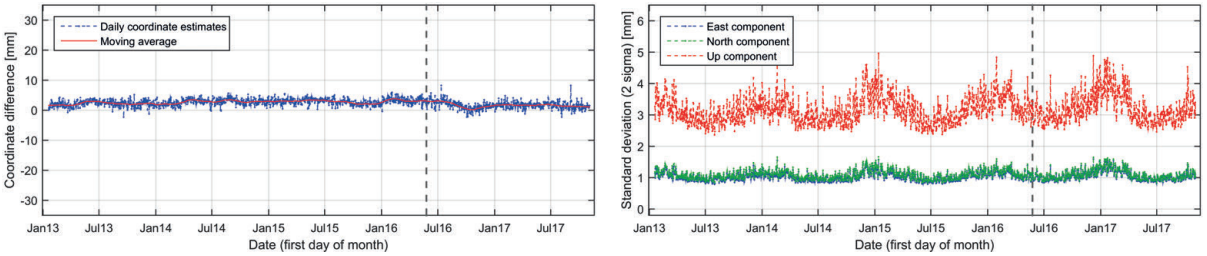

Figure 3.7: Coordinate differences (East component, left image) and coordinate standard deviations (right image) at site MENA with respect to the first observed day (18 January 2013); the dashed grey line marks the date of the CR deployment on 25 May 2016

ure 3.7, left image). This measure of coordinate variability is subsequently compared for the periods before and after the CRs were attached (2013-01-19 to 2016-05-24, and 2016-05-26 to 2017-11-04, respectively). The coordinate variability and a comparison of mean standard deviations for the periods before and after CR deployment are given in Table 3.1.

The difference in standard deviations between winter and summer months is much larger than the differences for the period before and after deployment (as seen in Figure 3.7, right image). In general, a slight increase of standard deviation and coordinate variability is observed after the CR deployment for all coordinate components (East, North and Up). However, the effect is less than 0.1 mm for all components and, therefore, negligible for long-term monitoring of surface displacements. More in-depth investigations in to multipath effects induced by the CRs could include using multipath stacking maps generated for a certain analysis period (e.g. Fuhrmann et al., 2015b).

Table 3.1: Statistical assessment of GPS coordinate variability at site MENA before and after CRs were deployed

Period	East	North	Up
Coordinate variability [mm]:			
before (1222 days)	0.70	0.63	3.20
after (527 days)	0.77	0.68	3.32
2σ standard deviation [mm]:			
before (1222 days)	1.04	1.09	3.15
after (527 days)	1.06	1.10	3.21

4 Conclusions

In this contribution, we have demonstrated the ability of InSAR to accurately measure surface displacements and displacement rates at a dense set of measurement points. The ability of satellite radar data to cover large areas presents a promising opportunity to include surface displacements detected by InSAR into national datums, particularly to update the vertical datum. In contrast to large-scale GNSS networks providing an accurate solution for continental plate tectonics, InSAR is well-suited to detect regional scale deformation phenomena. Future geodetic networks could make use of InSAR as a technique to densify geodetic measurements between existing GNSS sites in order to detect and characterise ground surface deformation at various spatial scales. Furthermore, InSAR can be used to frequently update coordinates of geodetic benchmarks affected by surface deformation without the need to directly take measurements on the ground at those benchmarks.

CRs can be deployed as part of geodetic monitoring networks in order to validate displacements measured by InSAR with displacements measured at the same location by GNSS or levelling. First results of the validation of InSAR and GPS observations from co-located geodetic monitoring sites reveal good agreement at the level of 5 to 10 mm. Co-located CR/GNSS sites may serve as a local tie to incorporate InSAR into national datums in the future. Validation and combination of InSAR with ground-based measurement techniques (such as GNSS or levelling) is important to account for the limitations of InSAR, which can include un-modelled atmospheric effects and the low sensitivity to North-South displacements. Statistical analysis of coordinate time series presented here has proven that potential GNSS multipath effects induced by CRs attached directly to GNSS monumentation have a negligible influence on daily site coordinates derived from GPS observations (below 0.1 mm).

The Sentinel-1 satellite mission launched in 2014 by European Space Agency (ESA) provides coverage of radar images over large areas with a generally short revisit time (usually 6 or 12 days). This creates the opportunity to use InSAR on a national scale in the future (Kalia et al., 2017). In compliance with ESA's new data policy (Aschbacher and Milagro-Pérez, 2012), Sentinel-1 data is provided completely free of charge. Therefore, it is possible to provide regular updates of InSAR deformation map products at a low cost once the data processing of the huge archive of Sentinel-1 data is streamlined and automated as far as practicable. National GNSS networks will help to link deformation maps derived at adjacent Sentinel-1 tracks and provide the opportunity to incorporate InSAR into the determination of vertical datums. InSAR analysis on a national scale will result in detailed and timely information on surface deformation to be used along with GNSS to update benchmark coordinates and to detect potential natural or anthropogenic deformation phenomena.

Acknowledgements

The authors would like to thank the Geological Survey of NSW, Department of Planning & Environment, for project funding and collaboration. We are grateful to all the property owners who provided access for the installation and usage of geodetic monitoring sites on their properties. We also want to thank all colleagues at Geoscience Australia involved in the construction of geodetic monitoring sites, GNSS survey campaigns, and analysis of GNSS and InSAR data. Many thanks to Josh Batchelor and Adrienne Moseley for internal review of the paper. This paper is published with the permission of the CEO, Geoscience Australia and the Executive Director, Geological Survey of NSW.

Persönlicher Gruß von Thomas Fuhrmann

Mehr als zehn Jahre lang hat Prof. Heck meinen beruflichen Werdegang begleitet und geprägt, zunächst als Student im Studiengang Geodäsie und Geoinformatik, später war er Hauptbetreuer meiner Doktorarbeit am Lehrstuhl für Physikalische und Satellitengeodäsie des KIT. Ich bedanke mich herzlich für die tolle Zusammenarbeit und die fachliche Unterstützung während meiner Zeit am "Lehrstuhl Heck". Seine positive und herzliche Art sowie sein konstruktives Feedback haben mich zu jeder Zeit motiviert die geodätischen Untersuchungen zu Oberflächenbewegungen im Oberrheingrabengebiet voranzutreiben, und schließlich maßgeblich zu meiner erfolgreichen Promotion am KIT beigetragen. Der obige Beitrag und die Tatsache, dass ich direkt nach meiner Promotion eine Stelle bei Geoscience Australia in Canberra antreten konnte, zeigen, dass das von Prof. Heck und Dr. Westerhaus geleitete und von mir bearbeitete DFG-Projekt zum Nachweis von Oberflächenbewegungen aus der Kombination verschiedener geodätischer Messtechniken (Nivellement, GNSS, InSAR) ein international aktuelles und praxisrelevantes Forschungsthema aufgegriffen hat. Vielen Dank für das mir entgegengebrachte Vertrauen und die Möglichkeit sowohl DFG-Projekt als auch Dissertation im Rahmen einer Vollzeitstelle als wissenschaftlicher Mitarbeiter durchzuführen. Ich wünsche Prof. Heck und seiner Frau alles Gute für den wohlverdienten Ruhestand und hoffe wir sehen uns bald wieder, in Deutschland oder Australien!?!

References

Adam, N., Kampes, B. M., Eineder, M., Worawattanamateekul, J., and Kircher, M. (2003): The Development of a Scientific Permanent Scatterer System. In: Schroeder, M., Jacobsen, K., and Heipke, C. (eds.) Proceedings of the Joint ISPRS/EARSeL Workshop "High Resolution Mapping from Space 2003", Hannover, Germany, 6–8 Oct 2003, pp. 1–6.

Altamimi, Z., Rebischung, P., Métivier, L., and Collilieux, X. (2016): ITRF2014: A new release of the International Terrestrial Reference Frame modeling nonlinear station motions. *Journal of Geophysical Research: Solid Earth* 121(8):6109–6131. DOI: 10.1002/2016JB013098.

Aschbacher, J. and Milagro-Pérez, M. P. (2012): The European Earth monitoring (GMES) programme: Status and perspectives. *Remote Sensing of Environment* 120:3–8. DOI: 10.1016/j.rse.2011.08.028.

Choi, D. C. T., Wong, J. Y. K., and Chan, B. S. B. (2007): Investigation on GPS Heighting Accuracy with the use of Hong Kong Satellite Positioning Reference Station Network (SatRef). In: Strategic Integration of Surveying Services, FIG Working Week 2007, Hong Kong SAR, China, 13-17 May 2007.

Dach, R., Lutz, S., Walser, P., and Fridez, P. (2015): Bernese GNSS Software Version 5.2 (User Manual). Astronomical Institute, University of Bern. Switzerland. ISBN: 978-3-906813-05-9.

Ferretti, A., Prati, C., and Rocca, F. (2000): Nonlinear subsidence rate estimation using permanent scatterers in differential SAR interferometry. *IEEE Transactions on Geoscience and Remote Sensing* 38(5):2202–2212. DOI: 10.1109/36.868878.

Ferretti, A., Prati, C., and Rocca, F. (2001): Permanent scatterers in SAR interferometry. *IEEE Transactions on Geoscience and Remote Sensing* 39(1):8–20. DOI: 10.1109/36.898661.

Fuhrmann, T. (2016): Surface Displacements from Fusion of Geodetic Measurement Techniques Applied to the Upper Rhine Graben Area. PhD thesis. Karlsruhe Institute of Technology, Germany. DOI: 10.5445/IR/1000056073.

Fuhrmann, T., Caro Cuenca, M., Knöpfler, A., van Leijen, F. J., Mayer, M., Westerhaus, M., Hanssen, R. F., and Heck, B. (2015a): Estimation of small surface displacements in the Upper Rhine Graben area from a combined analysis of PS-InSAR, levelling and GNSS data. *Geophysical Journal International* 203(1):614–631. DOI: 10.1093/gji/ggv328.

Fuhrmann, T., Luo, X., Knöpfler, A., and Mayer, M. (2015b): Generating statistically robust multipath stacking maps using congruent cells. *GPS Solutions* 19(1):83–92. DOI: 10.1007/s10291-014-0367-7.

Garthwaite, M. C., Nancarrow, S., Hislop, A., Thankappan, M., Dawson, J. H., and Lawrie, S. (2015): Design of Radar Corner Reflectors for the Australian Geophysical Observing System. Tech. rep. Geoscience Australia, Canberra, Australia.

Garthwaite, M. C. (2017): On the Design of Radar Corner Reflectors for Deformation Monitoring in Multi-Frequency InSAR. *Remote Sensing* 9(7). DOI: 10.3390/rs9070648.

Heck, B. (2003): Rechenverfahren und Auswertemodelle in der Landesvermessung. 3rd. Wichmann, Heidelberg, Germany.

Heckmann, B., Berg, G., Heitmann, S., Jahn, C.-H., Klauser, B., Liebsch, G., and Liebscher, R. (2015): Der bundeseinheitliche geodätische Raumbezug – integriert und qualitätsgesichert. *Zeitschrift für Vermessungswesen* 3/2015:180–184. DOI: 0.12902/zfv-0069-2015.

Hofmann-Wellenhof, B., Lichtenberger, H., and Wasle, E. (2008): GNSS – Global Navigation Satellite Systems. Springer, Vienna, Austria.

Hooper, A., Segall, P., and Zebker, H. A. (2007): Persistent scatterer interferometric synthetic aperture radar for crustal deformation analysis, with application to Volcán Alcedo, Galápagos. *Journal of Geophysical Research: Solid Earth* 112(B7):1–21. DOI: 10.1029/2006JB004763.

Hooper, A., Zebker, H. A., Segall, P., and Kampes, B. M. (2004): A new method for measuring deformation on volcanoes and other natural terrains using InSAR persistent scatterers. *Geophysical Research Letters* 31(23):1–5. DOI: 10.1029/2004GL021737.

ICSM (2017): Geocentric Datum of Australia 2020 Technical Manual Version 1.0. Tech. rep. Intergovernmental Committee on Surveying and Mapping, Australia.

Kalia, A. C., Frei, M., and Lege, T. (2017): A Copernicus downstream-service for the nationwide monitoring of surface displacements in Germany. *Remote Sensing of Environment* 202:234–249. DOI: 10.1016/j.rse.2017.05.015.

Kampes, B. M. (2005): Displacement parameter estimation using permanent scatterer interferometry. PhD thesis. Delft University of Technology, Delft, The Netherlands.

Li, J. and Heap, A. D. (2008): A Review of Spatial Interpolation Methods for Environmental Scientists. *Record 2008/23*. Geoscience Australia, Canberra, Australia, p. 137.

Parker, A. L., Featherstone, W. E., Penna, N. T., Filmer, M. S., and Garthwaite, M. C. (2017): Practical Considerations before Installing Ground-Based Geodetic Infrastructure for Integrated InSAR and cGNSS Monitoring of Vertical Land Motion. *Sensors* 17(8). DOI: 10.3390/s17081753.

Samieie-Esfahany, S., Hanssen, R. F., van Thienen-Visser, K., and Muntendam-Bos, A. (2010): On the effect of horizontal deformation on InSAR subsidence estimates. In: Lacoste, H. (ed.) Proceedings of Fringe 2009 Workshop, Frascati, Italy, 30 November – 4 December 2009, *ESA Publications SP-677*, pp. 1–7.

Torge, W. and Müller, J. (2012): Geodesy. 4th. de Gruyter, Berlin, Germany.